ACTIVE CONTROL FOR MICHELSON-STELLAR INTERFEROMETERS

John W. Hardy and Edward P. Wallner
Itek Corporation, Optical Systems Division, Lexington, Massachusetts, U.S.A.

ABSTRACT

The effects of atmospheric turbulence on the image structure in a ground based Michelson Stellar Interferometer are analyzed. A complete system requires compensation both for the wavefront distortions over the collecting apertures and for path length differences between them. Wavefront sensing and compensation have been previously described and analyzed. In this paper, a method of path length compensation and estimation of the mutual coherence function of the source is developed using matched filters in multiple spectral bands. A practical implementation of the resulting system is described and estimates of its performance given.

1. INTRODUCTION

The use of interferometry to measure the subtense of small objects and the separation of double stars was proposed by Fizeau in 1862, and first used by Michelson in 1890 to measure the diameters of Jupiter's Galilean satellites.

The method involves masking the telescope aperture to produce two slots whose separation can be varied. The interference fringes in the focal plane are observed as the slot spacing is changed. The fringe contrast is zero when the slot spacing A is $A_0 = \frac{B\lambda}{\theta}$, where λ = mean wavelength of observation, B = 0.5 for two point sources of angular separation θ, B = 1.22 for a uniform circular disk of angular diameter θ, and B > 1.22 for a circular disk with limb darkening. Thus θ may be determined by measuring the value of A_0 at which the fringe contrast disappears.

In 1920, Michelson and Pease extended this technique to slot separations much larger than the telescope aperture by mounting four mirrors on a 6-meter girder attached to the 100-inch Mount Wilson telescope. The two outer mirrors, whose separation was variable, collected the light from the object being

https://doi.org/10.1017/S025292110011869X Published online by Cambridge University Press

viewed and directed it to the inner mirrors which relayed the light into the telescope.

The location and contrast of the interference fringes produced by this apparatus depend not only on the brightness distribution of the object being measured, but also on wavefront disturbances produced by atmospheric turbulence and mechanical distortion of the optical structure. Manually operated optical compensators were used by Michelson to combat these effects, but of course these were only effective for slowly changing wavefront errors. The power spectrum of atmospheric turbulence normally extends to over 100 Hz. In spite of this problem, Michelson and Pease were able to measure the diameters of several large bright stars.

The main problem with the classical MI is the practical difficulty of making a quantitative measurement of fringe contrast and of accurately determining the null. The fringes are displaced, distorted and reduced in contrast by turbulence in the earth's atmosphere. The human eye is a very effective fringe detector because of its pattern-recognition capability, but is limited in sensitivity and speed of response.

Several workers have investigated photoelectric devices for fringe detection[1,2]. While sensitivity may be greatly improved with photon counting devices, the results have been limited by the random fringe distortion due to turbulence; considerable data processing is necessary to provide a useful signal-to-noise ratio. In 1967, Currie proposed a method of measuring the squared modulus of the mutual degree of coherence of the two beams, (γ^2) using a photon correlation technique[3]. The two beams are collimated and passed through a Köster prism where they are divided and interferometrically combined to produce two outputs. The fluctuations in the intensities of the two outputs are measured by photon-counting detectors and the number of auto-correlation (AC) and cross correlation (CC) events is determined using a correlation interval which is short compared with the time constant of the atmospheric fluctuations. Correlation events are counted over an integration time long enough to average out the modulation of the fringes by the atmosphere.

https://doi.org/10.1017/S025292110011869X Published online by Cambridge University Press

The fringe contrast is then given by

$$\gamma^2 = \left[\frac{2(AC-CC)}{AC+CC}\right]$$

This technique, termed "amplitude interferometry" allows a simpler detection scheme than the classic MI. However the measured values of γ^2 are degraded by local wavefront distortion across the collecting apertures and by path length differences comparable to the coherence length of the radiation. The latter effect gets more troublesome as the baseline of the interferometer increases.

There is much current interest in long baseline Michelson Stellar Interferometers, both to extend the capability of high angular resolution measurements beyond the $M_v = 2.5$ limit presently achieved by Intensity Interferometry[4] and also as the first step toward large coherent optical arrays[5].

While the use of non-redundant apertures reduces some of the effects of atmospheric turbulence in comparison with filled apertures, wavefront distortion is still the dominant limitation to the performance of ground-based MSIs. Local wavefront tilt and curvature across the individual collecting apertures may be compensated by a real time wavefront correction system such as RTAC[6] Such systems are capable of operating with bright reference stars, with a practical limit of 14th visual magnitude[7].

In this paper we briefly explore the important problem of fringe detection and show that active compensation of random path length differences provides a considerable improvement in the precision of fringe contrast measurement that is particularly valuable for long baseline interferometers.

2. SYSTEM MODEL

The basic interferometer model is shown in Fig. 1. The two collecting apertures are separated by a variable baseline A. The two beams are brought to a fixed separation D and focused by lens L onto the image plane X, where they overlap and interfere.

https://doi.org/10.1017/S025292110011869X Published online by Cambridge University Press

2.1 Ideal System

We first analyze an ideal system with no wavefront perturbations. The spectral intensity at the focal plane for a single rectangular aperture and an unresolved circular source is:

$$I_k = I_{ok} \operatorname{sinc}^2 \frac{kax}{F} \operatorname{sinc}^2 \frac{kby}{F} \tag{1}$$

where

$$I_{ok} = n_k \pi\alpha^2 \tau \frac{4a^2b^2k^2}{\pi^2 F^2} \tag{2}$$

$= $ Central spectral intensity in photons m^{-2} μm

n_k = Spectral radiance of source in photons $m^{-2}sr^{-1}s^{-1}\mu m$

α = Source angular radius in rd

τ = Exposure time in s

a = Half width of aperture in m

b = Half length of aperture in m

k = Wave number in μm^{-1}

$= 2\pi/\lambda$

F = Focal length of aperture in m.

Since the variation in intensity in the y direction, taken as normal to the line between the apertures, will not affect the fringe pattern being detected, any detectors may be assumed to extend over the entire pattern in this direction. This allows (1) to be integrated over y, reducing it to a function of x alone

$$I_{kx} = I_{okx} \operatorname{sinc}^2 \frac{kax}{F} \tag{3}$$

https://doi.org/10.1017/S025292110011869X Published online by Cambridge University Press

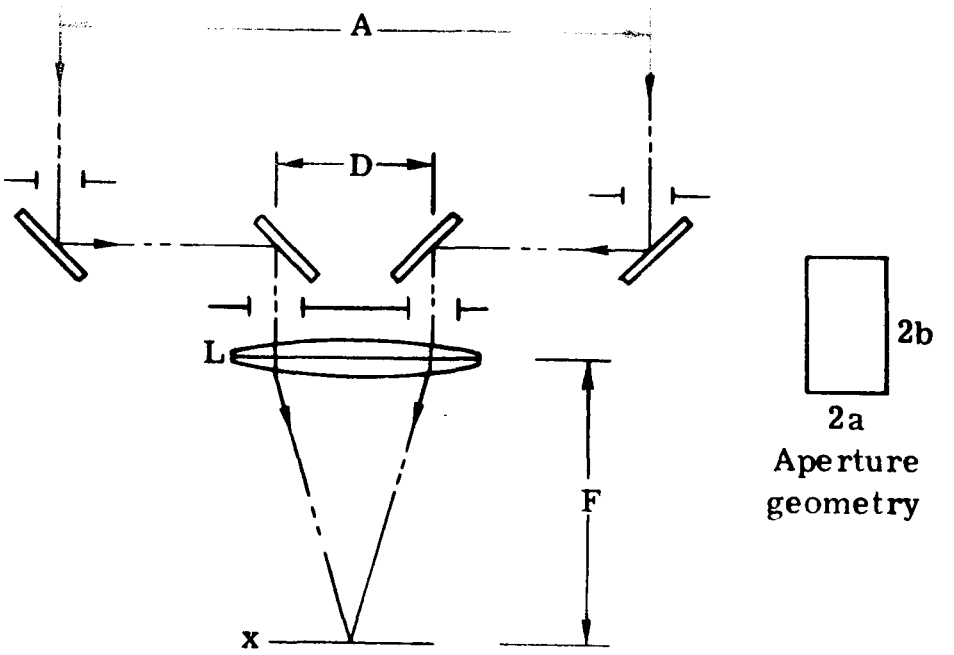

Fig. 1 — Interferometer model

$$L_x = 2I_0\,\gamma_W\,\mathrm{sinc}^2\,\frac{kax}{F}\left[1+\gamma_A\gamma_p\,\mathrm{sinc}\,\Delta k\left(\frac{Dx}{F}+\Delta p\right)\cos k\left(\frac{Dx}{F}+\overline{\Delta p}\right)\right]$$

γ_A = Fringe contrast due to object = $2J_1\,(k\alpha a)/k\alpha a$ for circular object

γ_W = Fringe contrast due to wavefront distortion σ_w

γ_p = Fringe contrast due to path length error Δp

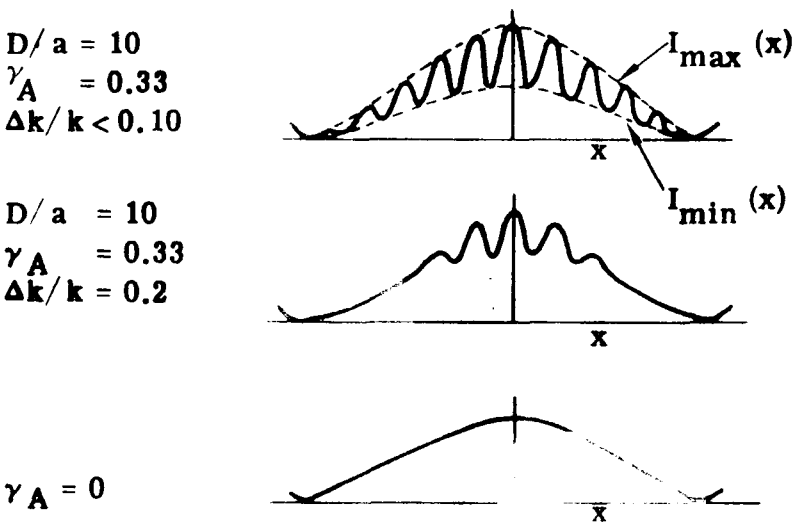

Fig. 2 — Interferometer image structure

https://doi.org/10.1017/S025292110011869X Published online by Cambridge University Press

Where

$$I_{okx} = n_k \pi\alpha^2\tau \frac{4a^2bk}{F} \tag{4}$$

If two such apertures separated by a distance D are focused at the same point and there are no phase disturbances, the spectral intensity becomes

$$I'_{kx} = 2I_{okx} \operatorname{sinc}^2 \frac{kax}{F} \left[1 + \gamma_A \cos \frac{kDx}{F}\right] \tag{5}$$

where γ_A = Normalized Fourier transform of object intensity distribution

$$= \frac{2J_1(k\alpha A)}{k\alpha A} \quad \text{for a circular source} \tag{6}$$

A = Baseline of interferometer in m.

For quasi-monochromatic light of wavenumber k, the interference fringes, defined by the cosine term, have a period of $2\pi F/kD$ in the image plane. For a circular source, the fringe contrast γ_A will fall to zero when $k\alpha A = 1.22\pi$ giving the classic result that the angular radius of the source is $\alpha = \frac{1.22\pi}{A_0 k}$

2.2 Spectral Bandwidth Effects

In the general case of wideband radiation from the source, the total intensity at position x is the integral over wavenumber of the spectral intensity given by (5);

$$I'_x = \int_0^\infty dk\, I'_{kx} \tag{7}$$

Let the radiation be restricted to a narrow but not necessarily "quasi-monochromatic" band:

$$\bar{k} - \Delta k < k < \bar{k} + \Delta k \tag{8}$$

https://doi.org/10.1017/S025292110011869X Published online by Cambridge University Press

I'_{okx} and γ_A will not change greatly over the spectral band if

$$\Delta k/\bar{k} \ll 1 \tag{9}$$

If $\text{sinc}^2 \frac{kax}{F}$ does not change greatly either, the integration in (7) reduces to:

$$I'_x \simeq 2I_{ox} \text{ sinc}^2 \frac{\bar{k}ax}{F} \left[1 + \gamma_A (\bar{k}) \cos \frac{\bar{k}Dx}{F} \text{ sinc } \frac{\Delta kDx}{F}\right] \tag{10}$$

where $I_{ox} = I_{okx}\, 2\Delta k$ = Intensity on axis.

The spectral bandwidth term $\text{sinc } \frac{\Delta kDx}{F}$ in (10) will reduce the fringe contrast to zero when

$$x = \frac{\pi F}{D\Delta k} \tag{11}$$

The assumption that $\text{sinc}^2 \frac{kax}{F}$ did not change greatly over the spectral band then implies

$$\frac{\Delta kax}{F} = \frac{\Delta ka}{F} \quad \frac{\pi F}{D\Delta k} \ll \pi$$

$$\text{or} \quad \frac{D}{a} \gg 1 \tag{12}$$

This condition is easily met and (10) can then be used to represent the total intensity distribution for the spectral band assumed.

The image structure for different spectral bandwidths and fringe contrasts is depicted in Fig. 2, for a D/a ratio of 10. Fig. 2(a) shows a narrow spectral band ($\Delta k/k < 0.1$) and non-zero fringe contrast; fringes appear across the entire image, the full number of fringes being D/a. Fig. 2(b) shows the same fringe contrast but a wider spectral band of $\Delta k/k = 0.2$; the (broadband) fringe contrast now drops to zero at half the image width. Using a wide bandwidth therefore enables the point of interferometer path length

https://doi.org/10.1017/S025292110011869X Published online by Cambridge University Press

equality to be determined, because only at this point are all wavelengths simultaneously in phase, resulting in the unique "white light" fringe. Fig. 2(c) shows the image structure for a wide spectral band when the fringe contrast is zero at the mean wavelength $\bar{k}$. In this case, fringe modulation still occurs at wavelengths higher and lower than the mean, suggesting that measurement of fringe modulation is best accomplished with a spectrally separated image.

2.3 Effects of Atmospheric Turbulence

Atmospheric turbulence produces three distinct effects on the interference image in a Michelson Stellar Interferometer. These effects are: 1) Differences in optical path length, from the object to the image, in the light collected by the two interferometer apertures; 2) Independent tilt of the two apertures, resulting in motion of the centroids of the two interfering images, so that the overlap area is reduced or eliminated; and 3) Wavefront curvature over each of the two apertures, resulting in spreading of the two images over a larger area.

In the central portion of the image, these effects may be accounted for by rewriting the expression for focal plane intensity distribution, Equation (10) as follows:

$$I'_x = 2I_{ox} \operatorname{sinc}^2 \frac{\bar{k} a x}{F} \gamma_w \left[1 + \gamma_A \gamma_k \gamma_p \cos \bar{k} \left(\frac{Dx}{F} + \Delta\bar{P}\right)\right]$$

where γ_k = Fringe contrast factor due to spectral bandwidth and cross product of bandwidth and mean path length error $\Delta\bar{P}$

$$= \operatorname{sinc} \Delta k \left(\frac{Dx}{F} + \Delta\bar{P}\right) \qquad (14)$$

γ_P = Fringe contrast factor due to time varying path length error ΔP

γ_W = Fringe contrast factor due to aperture wavefront error.

The function of the active control system is to optimize the values of γ_P and γ_W, in real time.

The magnitude and temporal characteristics of the turbulence effects will now be briefly summarized.

https://doi.org/10.1017/S025292110011869X Published online by Cambridge University Press

Atmospheric turbulence may be characterized by a Kolmogorov spectrum within its inertial sub-range defined by the inner and outer scales. The outer scale is limited by the height of the collecting aperture above the ground and may be typically only 1/5 of this distance[8]. Thus the baselines of ground-based interferometers having useful apertures (tens or hundreds of meters) will almost certainly be greater than the outer scale of the atmospheric turbulence, so that the path lengths to the two apertures may be considered statistically independent. The fluctuations in the path length differences will be dominated by disturbances being carried across each line of sight individually by the wind. In addition to these relatively rapid path length variations, there may be large-amplitude long-term fluctuations due to gross thermal effects.

To determine the temporal variation of optical path differences, the atmosphere can be treated as a series of "frozen" layers with varying wind velocities, allowing the frequency spectrum of phase errors to be computed, as has been done by Greenwood and Fried[9]. In the present paper, a single layer atmosphere corresponding to a uniform wind at all altitudes has been used to obtain order of magnitude results simply

The appearance of spectrally dispersed fringes under various conditions is shown in Fig. 3. Under ideal conditions, with exactly equal optical path lengths and with the object unresolved by the aperture spacing, the fringes will appear as in Fig. 3(a). The fringes at all wavelengths line up in the center of the image, producing the unique white light fringe. Under normal seeing conditions, the fringes are in constant motion and at one instant of time may appear as in Fig. 3(b). Even at path equality the fringes are randomly displaced in phase by atmospheric dispersion. Away from the null, the fringes get progressively more tilted. The direction of tilt reveals the polarity of the path length error.

The appearance of the dispersed fringes at path equality near the first null is shown in Fig. 3(c). As the interferometer aperture spacing is increased, the null first appears at the blue end of the spectrum and progresses through to the red end. The contrast γ_A at the edges of a band covering a 2:1

https://doi.org/10.1017/S025292110011869X Published online by Cambridge University Press

range of wavelengths spanning the null is about 40% at the red end and 15% at the blue end. It is therefore possible to maintain adaptive control over the interferometer path length even in the vicinity of the null. Note that the fringes change phase by π radians at the null, giving an unequivocal indication of the presence of a null.

2.4 Fringe Detection Performance

The operation of the interferometer depends on the ability to evaluate the term γ_A by measuring the fringe contrast in spite of the changes in fringe phase and the presence of the contrast degradation factors γ_P, γ_k and γ_W, caused by atmospheric and instrumental perturbations.

We require two outputs from the fringe detector:

(1) A path length error signal to feed back to the path length compensator to minimize ΔP.

(2) An estimate of the fringe contrast, γ_A, of the object observed.

The fringes may be detected by integrating the intensity after multiplying I'_x Equation (13) by orthogonal "matched filter" functions. Two signals result;

$$\left.\begin{aligned} C &= \int_{-\infty}^{\infty} dx \ \mathrm{sinc}^2 \frac{\bar{k}ax}{F} \ \mathrm{sinc} \frac{\Delta kDx}{F} \cos \frac{\bar{k}Dx}{F} \ I'_x \\ S &= \int_{-\infty}^{\infty} dx \ \mathrm{sinc}^2 \frac{\bar{k}ax}{F} \ \mathrm{sinc} \frac{\Delta kDx}{F} \sin \frac{\bar{k}Dx}{F} \ I'_x \end{aligned}\right\} \quad (15)$$

These spatial filters can be implemented either optically before detection, or electronically after detection. The latter more easily allows amplification of the signal before division between the filters, leading to lower quantum noise.

https://doi.org/10.1017/S025292110011869X Published online by Cambridge University Press

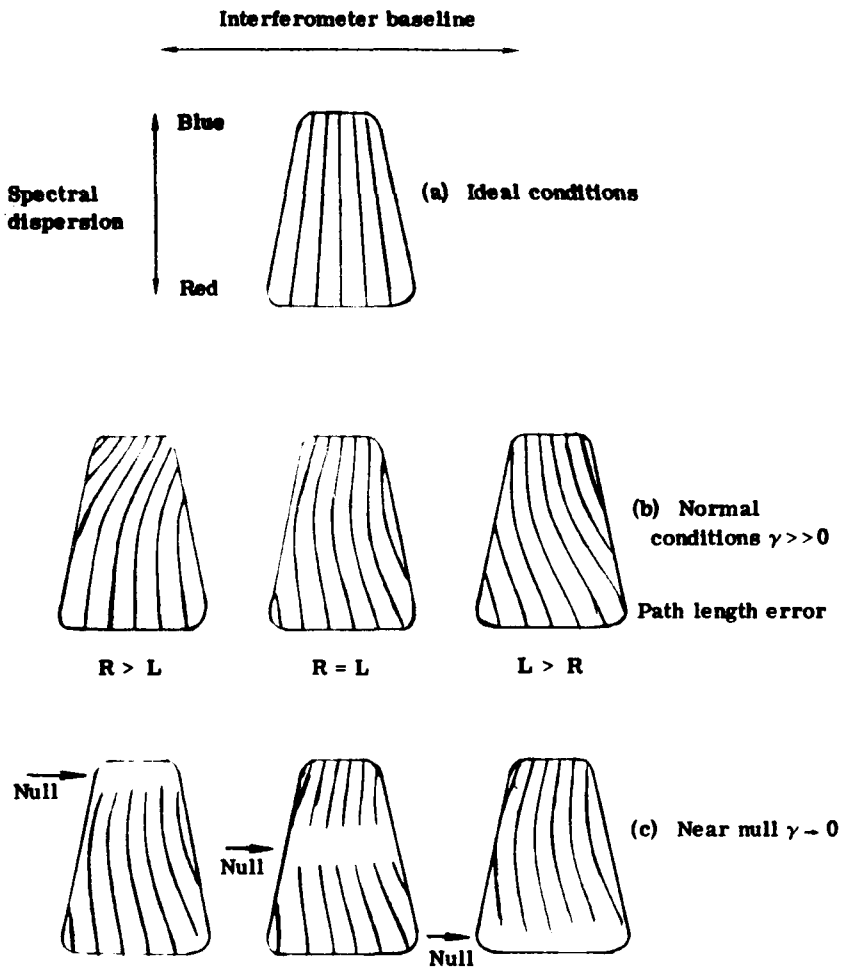

Fig. 3 — Fringe patterns with spectral dispersion

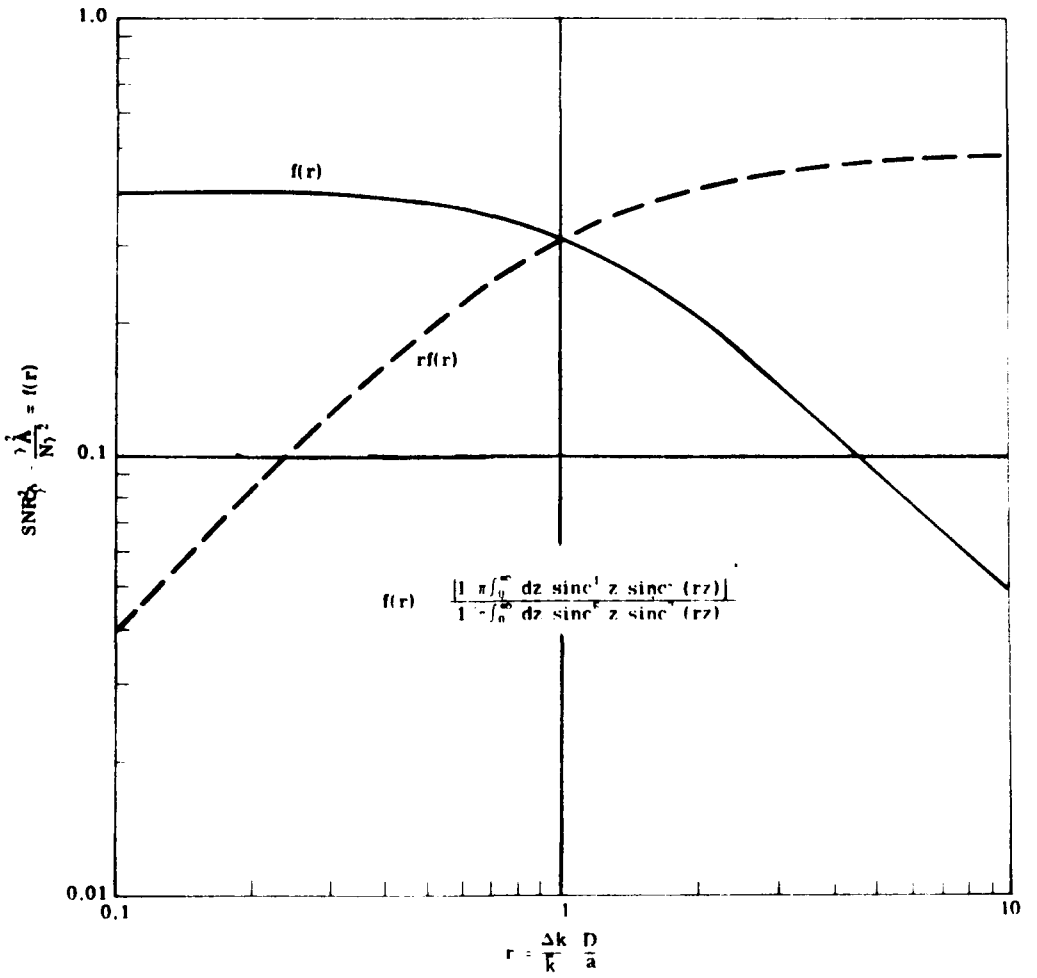

Fig. 4 — Normalized fringe detector performance

https://doi.org/10.1017/S025292110011869X Published online by Cambridge University Press

For the narrow wavenumber band considered, the fringe frequency terms may be averaged over one cycle giving

$$\left.\begin{aligned} C &= N\gamma_w\gamma_F \cos\phi\,(\bar{k})\; g_4\,(r) \\ S &= N\gamma_w\gamma_F \sin\phi\,(\bar{k})\; g_4\,(r) \end{aligned}\right\} \quad (16)$$

where N = total photons collected by both apertures in band Δk.

$$\gamma_F = \gamma_A\,\gamma_k\,\gamma_P \quad (17)$$

$$\phi(\bar{k}) = \bar{k}\,\Delta P \quad (18)$$

$$g_4(r) = \frac{1}{\pi}\int_0^\infty dz\ \mathrm{sinc}^4 z\ \mathrm{sinc}^2(zr) \quad (19)$$

$$z = \bar{k}\,a\,x/F \quad (20)$$

$$r = \frac{\Delta k}{\bar{k}} \cdot \frac{D}{a} \quad (21)$$

The fringe phase can now be estimated from the two filter outputs

$$\hat{\phi}(\bar{k}) = \tan^{-1}\,(S/C) \quad (22)$$

The variance of this estimate can be expressed as

$$\sigma^2_{\hat{\phi}} = \frac{1}{N\gamma_w\gamma_F^2}\,\frac{g_6(r)}{g_4^2(r)} = \frac{1}{N\gamma_N\gamma_F^2 f(r)} \quad (23)$$

Where $g_6(r) = \frac{1}{\pi}\int_0^\infty dz\ \mathrm{sinc}^6 z\ \mathrm{sinc}^2(zr)$ (24)

The function f(r) is plotted in Fig. 4. The number of photons collected is proportional to Δk which in turn is proportional to r, so that the signal-

https://doi.org/10.1017/S025292110011869X Published online by Cambridge University Press

to-noise ratio of the phase estimate is proportional to rf(r) which is also plotted on Fig. 4. Increasing the bandwidth reduces the variance of the fringe phase angle estimate linearly up to r = 1 and little thereafter. To avoid ambiguous phase measurements, the mean square fringe error should be limited to

$$\sigma^2_{\hat{\phi}} \leq (\pi/2)^2 \tag{25}$$

The path length error is given by

$$\hat{\Delta P} = \frac{1}{\bar{k}} \hat{\phi} \tag{26}$$

To reduce the path length error variance, the estimates from n equal wavenumber bands may be combined, giving

$$\sigma^2_{\hat{\Delta P}} = \frac{1}{\bar{k}^2 n} \sigma^2_{\hat{\phi}}$$

$$= \frac{1}{\bar{k}^2 \gamma_w \gamma_F^2 N f(r)} \tag{27}$$

Here nN is the total number of photons detected in all spectral bands. To minimize the path length error for a fixed spectral bandwidth $2n\Delta k$, one should minimize r. However, if r is too small, the photon error increases, violating the limit of equation (25). A good compromise is to choose

$$r \approx 1 \tag{28}$$

so that equation (27) becomes

$$\sigma^2_{\hat{\Delta P}} \approx \frac{3}{\bar{k}^2 n \gamma_w \gamma_F^2 N} \tag{29}$$

https://doi.org/10.1017/S025292110011869X Published online by Cambridge University Press

To summarize so far: we have established the performance of a method of fringe detection using matched filtering with spectrally separated bands. The estimate of fringe phase is defined by Equation (22), the resulting path length error is given by Equation (26) and the variance of the estimate is stated by Equation (29).

The next step is to make an estimate of the fringe contrast, which is done using the cosine and sine functions from (16)

$$\gamma^2_F = \frac{S^2 + C^2 - 2N\gamma_W g_6(r)}{\left[N\gamma_W g_4(r)\right]^2} \tag{30}$$

where N is the total number of photons collected.

The required value of γ_A may then be found using (17). The actual values of γ_k, γ_W and γ_P can be found from the residual errors of the active compensation system, which are discussed in section 3.

The rms error in the estimate of γ_A can be shown to be:

$$\sigma_{\hat{\gamma}_A} = \left[\gamma^2_k \gamma^2_P \gamma_W Nf(r)\right]^{-1/2} \tag{31}$$

which is the inverse of the mean square error in the fringe phase measurements at $\gamma_A = 1$.

It should be noted that the error in fringe contrast can be reduced by a large factor by averaging over an extended time period.

3. ACTIVE CONTROL SYSTEM

We now describe the practical implementation of a Michelson Stellar Interferometer using active control, based on the preceding ideas. The interferometer, shown in the block diagram Fig. 5, employs three separate servo control loops.

https://doi.org/10.1017/S025292110011869X Published online by Cambridge University Press

3.1 Baseline Control

The purpose of the first control loop is to maintain approximate equality of the mean optical path lengths in the two arms of the interferometer, while tracking the star and while varying the baseline. A suitable measurement technique is two-wavelength interferometry. Two axial beams are transmitted through the beamsplitters BS1 and BS2, traversing the baseline optics to the secondaries of the two collecting apertures T1 and T2 where they are retroreflected back through the system to the fringe-counting system. Optical path length differences are fed back to the path length corrector P1. The required bandwidth of this system is in the region of 10 Hz with a precision of about $\pm$ 10 micrometers. This baseline control system is also used to scan the optical path difference during initial acquisition of the star, in order to locate the central white-light fringe which is detected by the fringe signal processor Digital commands for baseline control will be provided in real time by the system computer.

3.2 Wavefront Compensation

The second active control system is an RTAC-type seeing compensator which provides both precise angle-tracking of the star and also compensation of wavefront distortion due to atmospheric turbulence. The essential features of this system, which has proven feasibility[6], are now briefly summarized.

The light bundles collected by the two apertures of the interferometer, which may be of any size or shape, are reduced optically to collimated beams about 5 cm across before being directed to the interferometer, where they are reflected off the deformable mirrors M1 and M2 to the objective mirror M3 which focuses the two images of the star at a common point on the grating G. Motion of the grating produces a periodic intensity modulation of the two beams which is picked up by the detector arrays D1 and D2 located at conjugate image planes of the deformable mirrors M1 and M2 Each detector element is related to a specific zone on the mirrors; the spacing of these zones at the telescope aperture is of the same order as r_0. The detector signals are demodulated by an array of phase detectors using a fixed phase reference generated by a light beam passing through the grating on the optical axis. Phase differences between

https://doi.org/10.1017/S025292110011869X Published online by Cambridge University Press

the fixed reference and each detector output signal produce error voltages which reveal the local tilt of the wavefront in each zone of the aperture. These local tilts are spatially integrated in the wavefront processor to form a complete map of the wavefront distortion. A parallel array of error signals is then fed back to the deformable mirror to compensate the distortion.

The residual wavefront error of such a system is composed of the following errors:

$$\sigma^2_W = \sigma^2_{FIT} + \sigma^2_\tau + \sigma^2_{PH} \tag{32}$$

The fitting error is due to the finite number of wavefront samples and correction zones in practical devices and has been analyzed by Hudgin[10]. For wavefronts generated by atmospheric turbulence, the fitting error is of the form

$$\sigma^2_{FIT} = \beta(L/r_0)^{5/3} \tag{33}$$

where L is the spacing of the correction zones

β is a constant depending on the shape of the response functions of the wavefront corrector.

The residual temporal wavefront error σ^2_τ is caused by changes in the wavefront over the finite integration time τ_w of the wavefront compensation system, which reduce the fringe contrast due to misalignment and spreading of the two overlapping images. This error may be expressed as

$$\sigma^2_\tau = 6.88 \left(\frac{b}{r_0}\right)^{5/3} \left[1.09 \left(\frac{V\,\tau_w}{b}\right)^{5/3} - 0.90 \left(\frac{V\,\tau_w}{b}\right)^2 \right] \tag{34}$$

The photon error σ^2_{PH} is a function of the number of photoelectrons M detected per subaperture in the wavefront sensor integration time τ_w. For an RTAC-type system the photon error is

$$\sigma^2_{PH} = \frac{2}{\gamma^2_w M} \left(\frac{L}{s}\right)^2 \tag{35}$$

where s = shear distance.

https://doi.org/10.1017/S025292110011869X Published online by Cambridge University Press

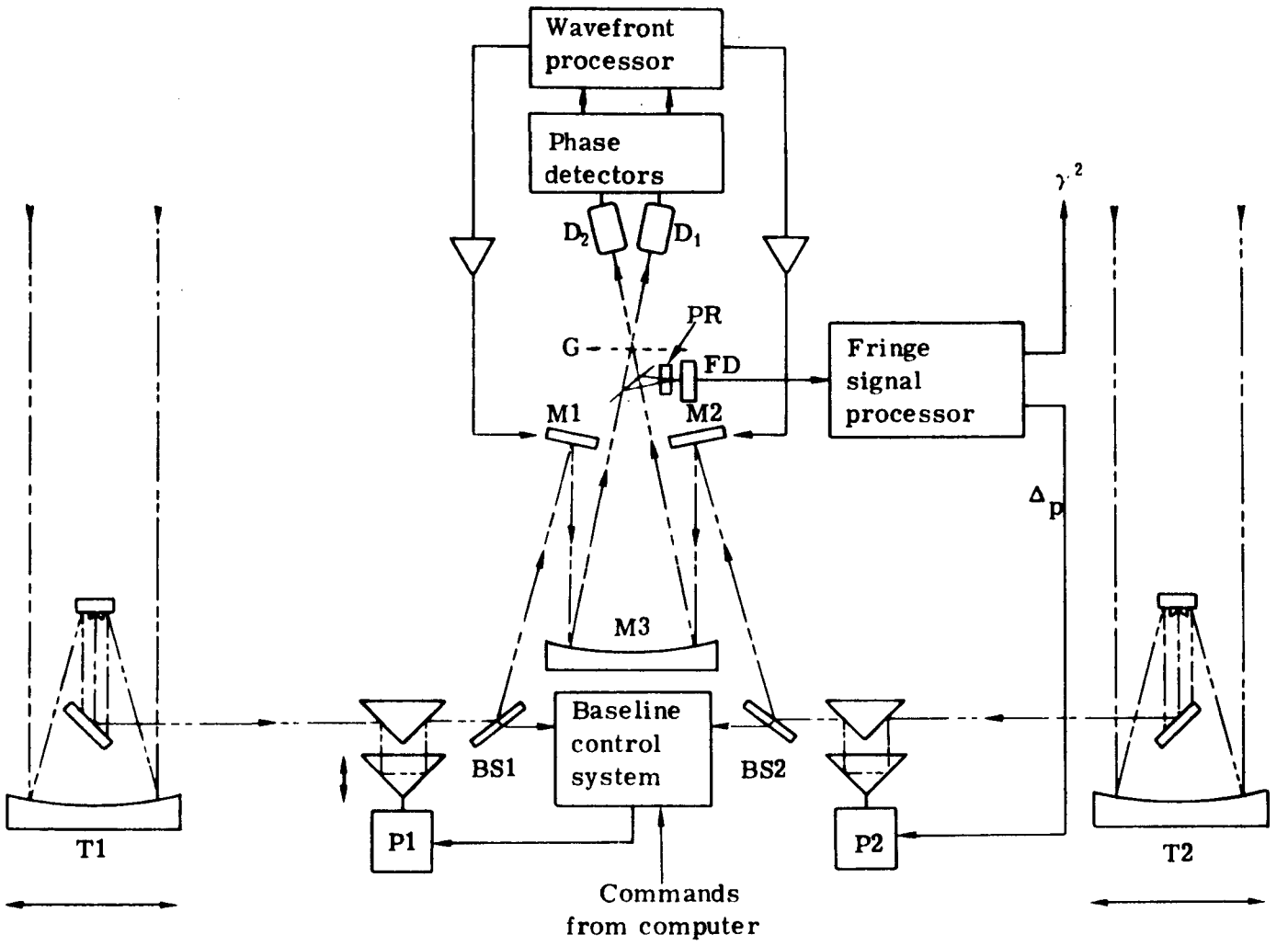

Fig. 5 — Active control system

https://doi.org/10.1017/S025292110011869X Published online by Cambridge University Press

The residual wavefront error σ^2_w may then be determined using Equation (32). The fringe contrast factor γ_w may be found for small values of σ_w by using the Strehl ratio:

$$\gamma_w = e^{-\sigma^2_w} \tag{36}$$

The integration time τ_w appears in the numerator of Equation (34) and in the denominator of Equation (35) (through both γ_w and M). The value of τ_w must therefore be optimized to maximize some aspect of system performance.

3.3 Path Length Compensation

The third active control system is the fringe tracker which compensates the optical path length difference due to the atmosphere in real time to maintain the phase of the fringes within $\pm$ 1/2 wavelength. This is an essential part of the system especially for long baseline interferometers, because without fringe tracking the uncompensated path length error due to the atmosphere is so great that the spectral bandwidth necessary to obtain the required coherence length becomes impractically small[4].

The essential components of the fringe tracking system are the prism PR, the detector array FD, and the fringe signal processor shown in Fig. 5 Part of the light forming the superimposed star images is diverted by a beamsplitter through the prism to form a spectrally dispersed image on the detector array. Spectral dispersion of the image using a prism has the advantage that it is optically simple and efficient. The main disadvantage is that the spectral resolution is limited by the width of the diffraction image of the interferometer aperture normal to the baseline. Maximizing the aperture in this direction is therefore beneficial as it not only increases the collected light but also concentrates it in a smaller area.

The configuration of the detector array FD is shown in Fig. 6. Each row of elements corresponds to one of the n spectral bands; in the diagram, n = 5. The detector geometry matches the fringe spacing, which varies with wavelength. The fringes are sampled by four detector elements per cycle. The number of

https://doi.org/10.1017/S025292110011869X Published online by Cambridge University Press

fringes in the X direction is approximately D/a, so that the total number of detector elements is 4nD/a. For a D/a ratio of 5, there are 20 detector elements per row. A flow diagram of the signal processing required to obtain the estimates of fringe phase and contrast is shown in Fig. 7 The first operation is to correlate the image samples ΔI_x with the matched filter functions $\left[W(x)\cos Gx\right]$ and $\left[W(x)\sin Gx\right]$, summing them over the X-dimension of the image to form the outputs S and C, from which the fringe phase estimates $\hat{\phi}$ are made for each spectral band. These estimates are then averaged and multiplied by $1/\bar{k}$ to give the path length error $\hat{\Delta P}$, which is fed back to the high-speed path length corrector P2 to close the fringe tracking loop.

The dominant error in path length estimation, σ^2_P is due to changes in the aperture averaged wavefront over the finite integration time τ_P during which the measurement is made.

It may be shown that the temporal path length error due to atmospheric turbulence is

$$\sigma^2_P = 12.4 \left[\frac{r_0}{b}\right]^{1/3} \left[\frac{V\ \tau_P}{r_0}\right]^2 \qquad (37)$$

where σ^2_P = mean square path length error at mean wavelength (radians)^2

b = aperture radius

V = wind velocity

r_0 = Fried's coherence length

This residual path length error depends only weakly on aperture size, but is directly proportional to the integration time and wind velocity. The resulting fringe modulation factor is approximated by

$$\gamma_P = e^{-\sigma^2_P} \qquad (38)$$

https://doi.org/10.1017/S025292110011869X Published online by Cambridge University Press

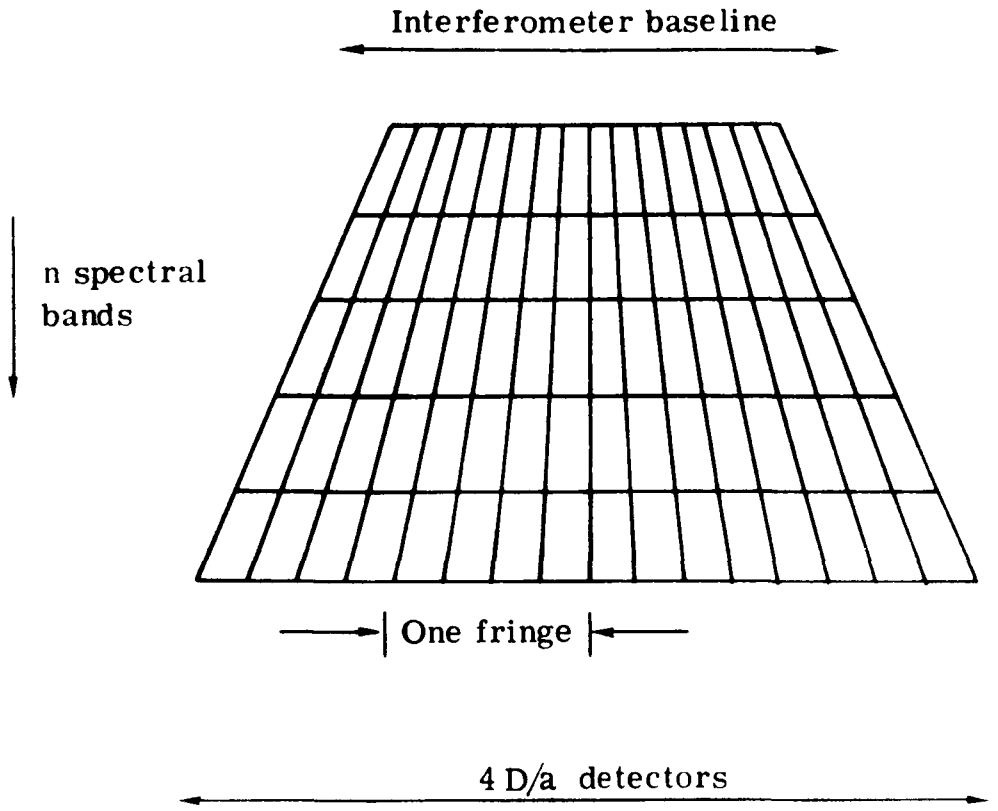

Fig. 6 — Detector array

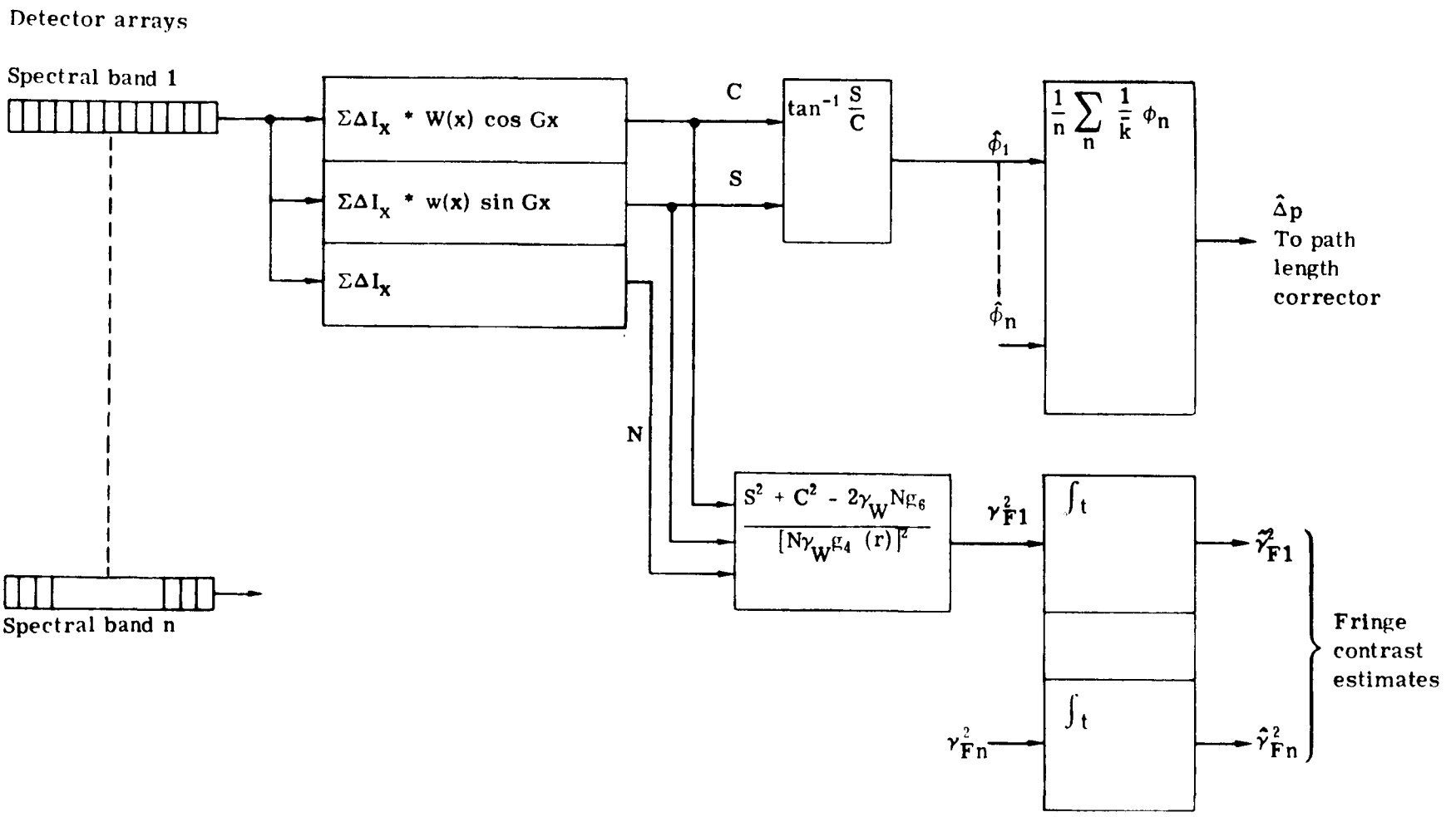

Fig. 7 — Fringe detector signal processor

https://doi.org/10.1017/S025292110011869X Published online by Cambridge University Press

3.4 Fringe Contrast Estimation

The overall fringe contrast γ_F is found using equation (30). The functions C and S have already been formed. The intensities of all detector outputs in the row are summed to obtain $N\gamma_w$, from which the functions $2N\gamma_w g_6(r)$ and $N\gamma_w g_4(r)$ are formed. The estimates of γ_F^2 are then computed for each spectral band and time averaged. The final step is to compute the required output of the system, which is the object mutual coherence function γ_A, using equation (17). With active control of path length, ΔP will be small and γ_k will consequently be close to unity. The values of γ_w and γ_P are obtained from the measured wavefront error σ_w and path length error σ_P, using equations (36) and (38)

4. SYSTEM PERFORMANCE

The performance of the active interferometer described has been estimated based on the use of an RTAC system, assuming the following parameters

Atmospheric coherence length	$r_0 = 10$ cm
Wind velocity	$v = 5$ m s^{-1}
Telescope aperture size	= 5 x 5 subapertures
Aperture ratio D/a	= 5
Shear distance	= Subaperture size

The photometry has been based on a type G star assuming an overall optical transmission of 50% to the wavefront sensor detectors D1 and D2 and 25% to the fringe detector FD. S-20 detectors have been assumed.

4.1 Wavefront Compensation

The residual error σ^2 has been computed using equations (32) through (36). Several system parameters in these equations may be chosen to optimize some aspect of system performance. Here the parameters have been chosen to maximize the visual magnitude of the dimmest source for which the corrector can lock on and correct.

https://doi.org/10.1017/S025292110011869X Published online by Cambridge University Press

The subaperture size is chosen to maximize the value of $(S/r_0)^2 e^{-2\sigma^2_{FIT}}$, assuming the shear S equals the subaperture size L. This leads to a value of $L = 1.214\ r_0$.

The wavefront integration time τ_w is chosen to maximize the value of $(V\tau_w/b)\ e^{-2\sigma^2\tau}$. For a ratio of $b/r_0 = 2.5 \times 1.214 = 3.0$ the maximum occurs at $V\tau_w/b = 0.0645$ giving $\tau_w = 3.9 \times 10^{-3}$ second.

Similarly, there is an optimum value of σ^2_{PH}, which occurs at $\sigma^2_{PH} = 0.5$. These optimized values have been used to obtain the wavefront error σ^2_w and the corresponding fringe contrast γ^2_w which are plotted vs. visual magnitude in Fig. 8. The fringe contrast is seen to remain relatively high until the limiting magnitude of $M_v = 7.4$ is approached.

4.2 Fringe Detection

The spectral response of the source, atmosphere and detector extends from 0.4 to 0.6μm giving $\Delta k/k = \Delta\lambda/\bar{\lambda} = 0.1/0.5 = 0.2$. This gives a value of $r = (D/a)(k/Dk) = 1$ using a single spectral band in the fringe detector.

The detector integration time is chosen to maximize $(V\tau/r_0)e^{-2\sigma^2_p}$. The resulting value of $V\tau/r_0 = 0.17$, or $\tau = 3.4 \times 10^{-3}$ seconds.

These parameter values can now be substituted in equation (23) to evaluate the error in fringe phase estimation, at the limiting magnitude, which is $\sigma_{\hat{\phi}} = 0.116/\gamma_A$. The fringe contrast γ_A required to keep the rms phase error less than $\frac{\pi}{2}$ is therefore 0.074.

At the limiting magnitude, the rms error in fringe visibility for a single integration period is $\sigma_{\hat{\gamma}} = 0.116$. This can be reduced to 0.01 by integrating the estimates over a period of 0.5 seconds.

The performance using fixed system parameters for sources brighter than the limiting magnitude is shown in Fig. 9. Both phase and γ_A errors fall rapidly as magnitude is decreased allowing the measurements to be made more accurately, more rapidly, or at lower values of γ_A.

https://doi.org/10.1017/S025292110011869X Published online by Cambridge University Press

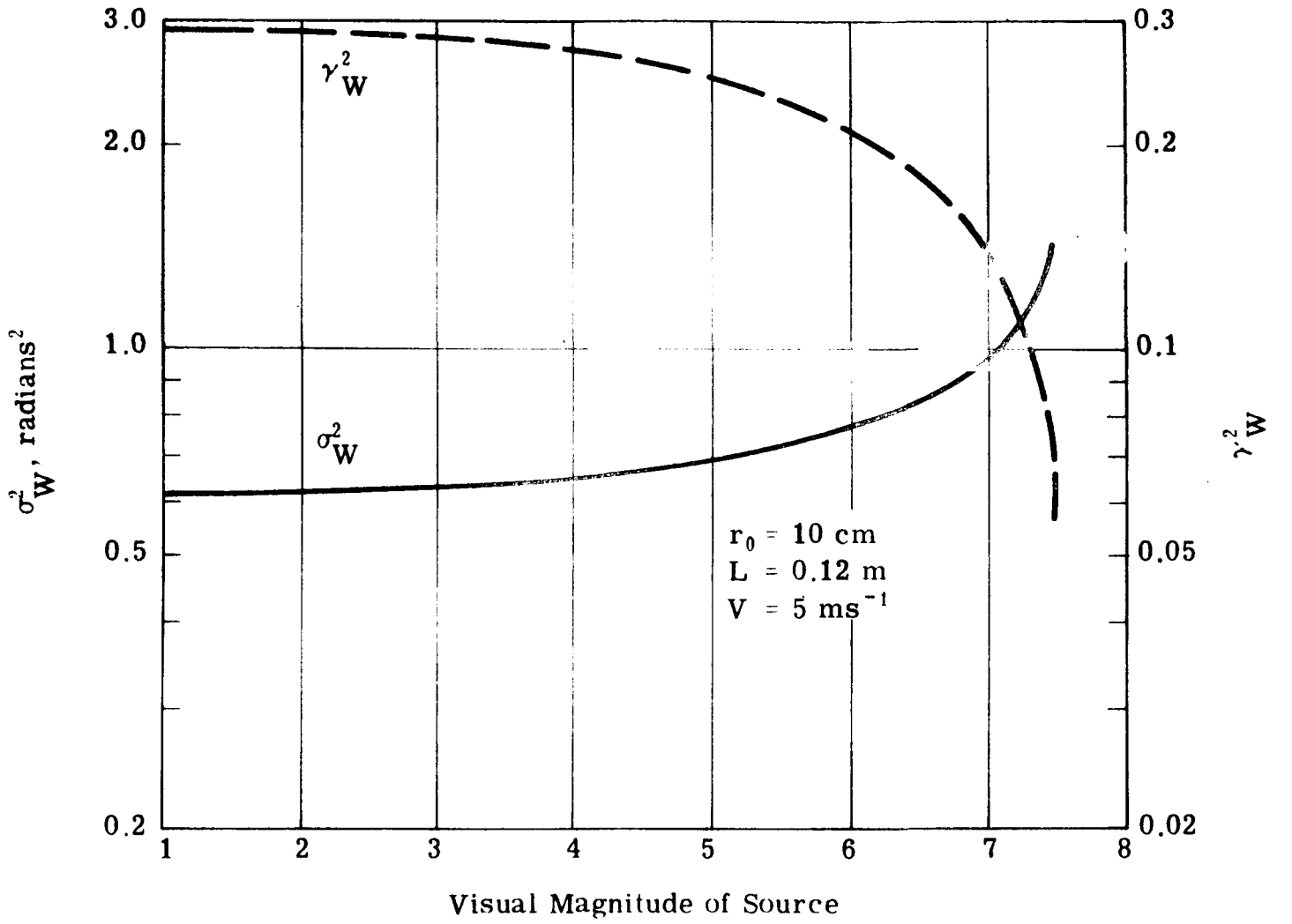

Fig. 8 — Wavefront error versus magnitude

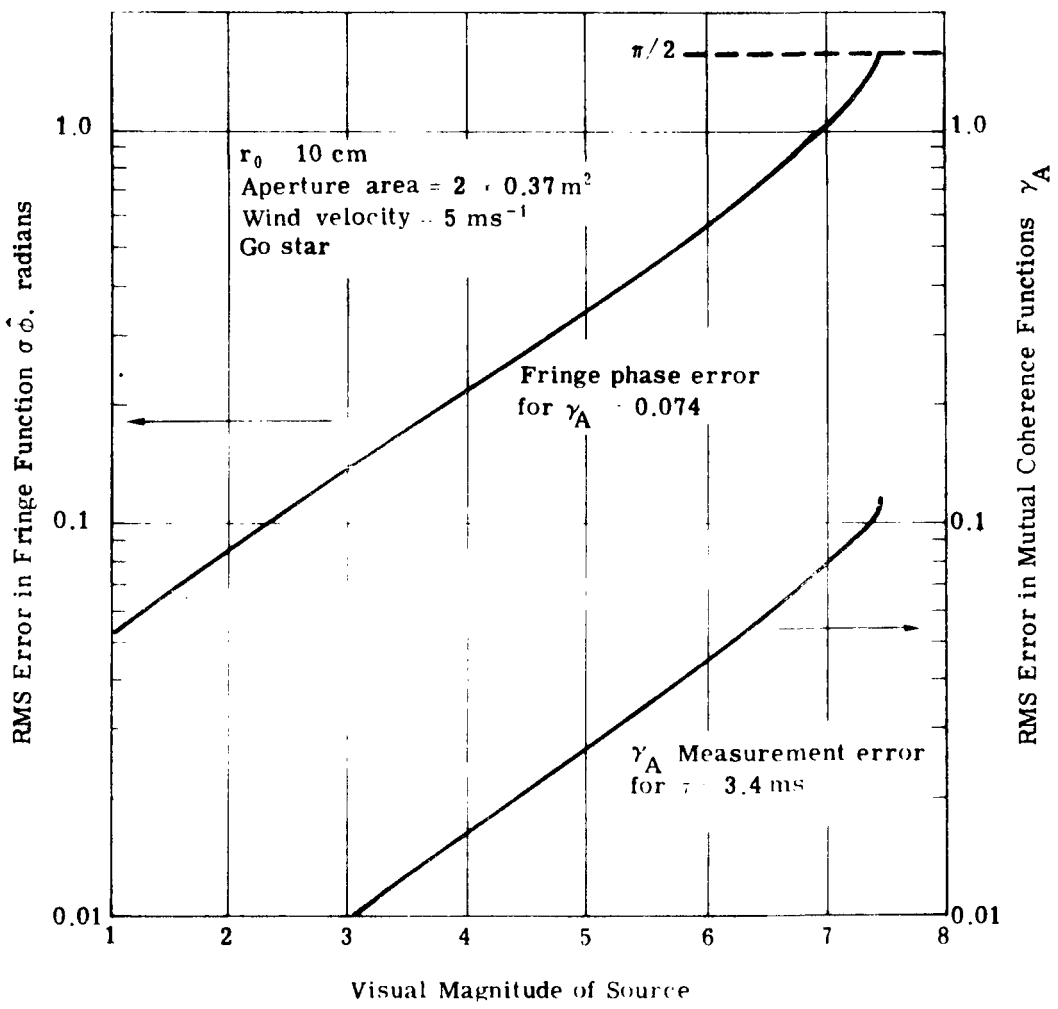

Fig. 9 — System performance

https://doi.org/10.1017/S025292110011869X Published online by Cambridge University Press

Conclusions

The use of active control to compensate atmospheric wavefront distortion and path length errors in a Michelson Stellar Interferometer provides an instrument whose performance is not limited by baseline length, allowing baselines of a kilometer or more.

The modulus of the mutual coherence function may be measured with an error of 1% using an integration time of the order of a second with modest apertures.

The performance of such a system depends on the detector technology available, and with current technology Go stars to visual magnitude 7.4 can be used. This means that approximately 20000 stars in the SAO catalog would be within the range of the instrument.

REFERENCES

1) W.I. Beavers and W.D. Swift, Photoelectric Fringe Strength Measurement, Applied Optics, 7, 1975-1979 (1968).

2) J.L. Elliott and I.S. Glass, A Quantitative Fringe Detector for Stellar Interferometry, The Astronomical Journal, 75, 1123-1132, (1970).

3) D.G. Currie, S.L. Knapp and K.M. Liewer, Four Stellar-Diameter Measurements by a New Technique: Amplitude Interferometry. The Astrophysical Journal, 187, 131-134, 1974.

4) R. Hanbury Brown, Intensity Interferometry versus Michelson Interferometry, Proceedings of ESO Conference on Optical Telescopes of the Future, Cern, Geneva, 391-407, Feb. 1978.

5) A. Labeyrie, Interference fringes obtained on Vega with two optical telescopes, The Astrophysical Journal, 196, L71-L75, 1975.

6) J.W. Hardy, J.E. Lefebvre and C.L. Koliopoulos, Real time atmospheric compensation, J.Opt.Soc.Am., 67, 360-369, 1977.

7) F.J. Dyson, Photon noise and atmospheric noise in active optical systems, J.Opt.Soc.Am., 65, 551-558, 1975.

8) R.S. Lawrence and J.W. Strohbehn, A Survey of Clear-Air Propagation Effects Relevant to Optical Communications, Proc IEEE, 58, 1523-1545, 1970.

9) D.P. Greenwood and D.L. Fried, Power spectra requirements for wave-front compensative systems, J.Opt.Soc.Am., 66, 193-206, 1976.

10) R.H. Hudgin, Wavefront compensation error due to finite corrector-element size, J.Opt.Soc.Am., 67, 393-395, 1977.

https://doi.org/10.1017/S025292110011869X Published online by Cambridge University Press

DISCUSSION

R.Q. Twiss: The system proposed here is certainly very attractive, but I think that one might be able to reach to a fainter limiting magnitude, say +9, by using longer integration times and smaller apertures. In this case you only have to correct for tilt and use a relatively slow path compensator. This method would require longer integration times, but is much simpler.

J.W. Hardy: Reducing the size of the apertures to a single element of size r_o would have little effect on the limitng magnitude of the RTAC system because the wavefront tilt is already measured and corrected over subapertures of this size, using parallel detectors and feedback channels. The performance is essentially independent of the total number of subapertures (assuming that they are of constant size). The integration time is determined mainly by wind speed.

In the fringe tracker, we have a different situation because we use the light collected by the entire aperture. Our calculations indicate that apertures appreciably greater than 10 cm in diameter are required in order to provide a signal to noise ratio which can keep the fringe error less than $\pm\pi/2$ at the limting magnitude of the RTAC system. The aperture size is therefore determined mainly by the fringe tracking requirement.

R.Q. Twiss: If you don't require perfect correction of the errors and accept the resulting loss in contrast, and if you measure the errors by auxiliary means, then one should be able to get to faint stars with the smaller apertures.

E.P. Wallner: Yes, it turns out that for an optimum system the contrast has a fairly low value.

K.M. Liewer: How sensitive is the system to scintillation?

J.W. Hardy: Scintillation will decrease the number of photons collected by either or both apertures. For equal scintillation at the two apertures, this leads to a sensitivity loss which is simply proportional to the light loss. When the scintillation is unequal, then some loss of fringe contrast will occur. We have not yet evaluated the effect of this on system performance.

https://doi.org/10.1017/S025292110011869X Published online by Cambridge University Press

E.P. Wallner: Fried mentioned that the scintillation of starlight is only a few percent, and the sensitivity reduction should be of the same order of magnitude.

https://doi.org/10.1017/S025292110011869X Published online by Cambridge University Press